Journal of Biomedical Optics 9(5), 951–960 (September/October 2004)

Differential oblique angle spectroscopy of the oral epithelium

David Hattery
National Institutes of Health
National Institute of Child Health and Human Development
Laboratory of Integrative and Medical Biophysics
Building 9, Room B1E11
Bethesda, Maryland 20892-0924
E-mail: hattery@ieee.org

Brenda Hattery
Apogee Biodimensions
5630 16th St NW
Washington, D.C. 20011-6810

Victor Chernomordik
National Institutes of Health
National Institute of Child Health and Human Development
Laboratory of Integrative and Medical Biophysics
Building 9, Room B1E11
Bethesda, Maryland 20892-0924, USA

Paul Smith
National Institutes of Health
Office of Research Services
Bethesda, Maryland 20892

Murray Loew
George Washington University
Department of Electrical and Computer Engineering
Washington, D.C. 20052

James Mulshine
National Institutes of Health
National Cancer Institute
Bethesda, Maryland 20892

Amir Gandjbakhche
National Institutes of Health
National Institute of Child Health and Human Development
Laboratory of Integrative and Medical Biophysics
Building 9, Room B1E11
Bethesda, Maryland 20892-0924

Abstract. Increasing evidence suggests that inflammation may contribute to the process of carcinogenesis. This is the basis of several clinical trials evaluating potential chemopreventive drugs. These trials require quantitative assessments of inflammation, which, for the oral epithelium, are traditionally provided by histopathological evaluation. To reduce patient discomfort and morbidity of tissue biopsy procedures, we develop a noninvasive alternative using diffuse reflectance spectroscopy to measure epithelial thickness as an index of tissue inflammation. Although any optical system has the potential for probing near-surface structures, traditional methods of accounting for scattering of photons are generally invalid for typical epithelial thicknesses. We develop a single-scattering theory that is valid for typical epithelial thicknesses. The theory accurately predicts a distinctive feature that can be used to quantify epithelial thickness given intensity measurements with sources at two different angles relative to the tissue surface. This differential measure approach has acute sensitivity to small, layer-related changes in scattering coefficients. To assess the capability of our method to quantify epithelial thickness, detailed Monte Carlo simulations and measurements on phantom models of a two-layered structure are performed. The results show that the intensity ratio maximum feature can be used to quantify epithelial thickness with an error less than 30% despite fourfold changes in scattering coefficients and 10-fold changes in absorption coefficients. An initial study using a simple two-source, four-detector probe on patients shows that the technique has promise. We believe that this new method will perform well on patients with diverse tissue optical characteristics and therefore be of practical clinical value for quantifying epithelial thickness *in vivo*. [DOI: 10.1117/1.1781161]

Keywords: oral; cancer; spectroscopy; inflammation; diffuse reflectance; chemopreventive.

Paper 03089 received Jul. 2, 2003; revised manuscript received Dec. 10, 2003; accepted for publication Jan. 21, 2004.

1 Introduction

We have developed a simple and inexpensive technique for noninvasively quantifying the thickness of the oral epithelium. Inflammation of the oral epithelium can provide a promotional environment that drives the progression of early cancer cells.[1–3] A key step in the inflammation response of epithelial tissue is the generation of the enzyme cyclooxygenase (Cox). Increased Cox activity leads to the production of prostaglandin E2 (PGE2) and recruits inflammatory cells back into the area surrounding the PGE2 release. It has been proposed that the release of inflammatory cell products in that focal area of tissue injury results in the growth stimulation of both normal cells as well as evolving early cancer cells.[2]

New chemopreventive drugs that inhibit Cox production and lead to decreases in PGE2 levels are now available.[4,5] If these anti-inflammatory drugs are useful in reducing the numbers of inflammatory cells there would be a reduction in number and therefore volume of the local, hyperproliferative normal epithelial cells. The epithelial response is typically determined by tissue biopsy. In the relatively small oral compartment, however, repeated surgical biopsy procedures are traumatic. This invasive procedure can cause patient discomfort and morbidity, which limits the options for repeat measurements to monitor patient progress. Thus, a noninvasive procedure is desired.

Information on numerous aspects of a tissue milieu and its biochemistry is contained in visible light spectra. The reflected light from a tissue surface, however, depends not only

Address all correspondence to Dr. David W. Hattery, National Inst. of Health, 5630 16th St NW, Washington, D.C. 20011-6810, USA. Phone: 202-726-1994; Fax: 202-726-0007; E-mail: hattery@ieee.org

1083-3668/2004/$15.00 © 2004 SPIE

on the absorption spectrum of the analytes, but also on the scattering properties of the tissue under investigation. Tissue is highly scattering and the epithelium can be several scattering distances thick. Researchers have developed approximate analytical solutions for photon migration in layered media based on the diffusion approximation to transport theory[6–11] or random walk theory[12–14] (RWT). Neither of these techniques is suitable for extracting the thickness of or the optical properties of a thin epithelial layer using diffuse reflectance measurements.

Confocal microscopy and optical coherence tomography (OCT) have been used to image the structure of the skin[15] and oral epithelium.[16,17] Others have developed models for photon migration to obtain spectroscopy data for functional studies of the skin and underlying muscle.[18] Usually the top layer is considered a confounding influence that distorts measurements of the underlying tissue properties.[8–11] Models based on RWT have been developed for thick layered media and the statistics of diffuse reflectance photons have been characterized.[12–14] A different photon migration model is desired, however, for extracting spectroscopic values principally for a thin upper layer, such as the epithelium.

Optical reflectance spectroscopy has been used to quantify tissue oxygenation levels near the exposed surface of myocardium of the porcine heart *in vivo* by Gandjbakhche et al.[19] and Arai et al.[20] at the National Heart, Lung, and Blood Institute (NHLBI) at the National Institutes of Health. Monte Carlo (MC) simulations performed by Gandjbakhche et al.[19] indicate that in the 520- to 590-nm range, the mean path length within the myocardium for diffusely reflected light varies from 1.2 to 1.4 mm, while the mean penetration depth into the epicardium is between only 330 and 400 μm for blood-free heart tissue. From this project, several conclusions can be drawn. First, in oblique angle reflectometry, the penetration depth of photons in the visible spectrum where the blood absorption is high did not exceed 1 mm; additionally, MC simulations and subsequent theoretical analysis showed that, in such a highly absorptive medium, the mean maximum penetration depth is twice the mean depth.[19]

This means that the detected photons are mainly those that reverse direction only once; while the photons may experience numerous small-angle scatterings, there is only one large-angle scattering. Furthermore, shallow insertion angles result in less penetration depth, and these enable one to use scattering theories based on integral equations to model light migration up to 1 mm below the tissue surface.

Normal oral epithelium is approximately 0.1 mm thick. Chronic inflammation, however, may increase the thickness of the epithelial layer to as much as 0.5 mm. This observation, combined with OCT imaging showing the optical differentiation at the boundary between the epithelial layer and the stroma,[16] led to the conclusion that the thickness of the epithelium could be quantified using diffuse reflectance spectroscopy (DRS). A DRS device would have the advantage of providing a single measure of epithelial thickness using a simple and inexpensive probe. By comparison, OCT provides an image that would then require an evaluation by a trained individual to interpret the location of the layer boundary, and hence layer thickness.

From the earlier results obtained by Gandjbakhche et al.,[19] it followed that for specific scattering and absorption conditions, a simple single-reverse-scattering model can be used to locate the epithelial boundary position up to 1 mm below the surface. This simplification, combined with the noninvasiveness of DRS, substantiates the conclusion that quantification of oral epithelium thickness was a good DRS application and could have a rapid progression from desk, to bench, to bedside. A single-scattering model was built and tested against MC simulations and phantoms.[21] An analysis of these results is presented both to show the method can quantify layer thickness and to provide rough bounds on the accuracy of the method. As part of the bench-to-bedside progression, results are also presented from an initial clinical study using a simple two-source, four-detector probe that show the method is not adversely effected by the heterogeneity of patient tissue. These tests indicate the DRS approach has the potential to provide useful measurements of epithelial tissue thickness.

2 Theory

The epithelium and stroma have different scattering and absorption properties; specifically, the epithelium has higher scattering and the stroma has a greater concentration of light-absorbing hemoglobin due to increased vascularization. This layered structure results in a perturbation of the photon intensity falloff with increasing source-detector separation that can be used to determine the depth of the boundary between the epithelium and stroma.

An analytical model was devised, using integral equations, to describe the propagation of photons inserted into layered tissue at a specific oblique angle for which a large-angle scattering event results in their detection at some radial distance from their insertion point. The scattering geometry for a single large-angle scatter for two insertion angles is illustrated in Fig. 1.

In general, the intensity detected at a detector at a given radial distance r from the insertion point can be written as follows:

$$I_d(r) = I_0\left[\sum_{\text{all1spaths}} p_{s1}p_{\text{ns2}a}p_{\text{ap}} + \sum_{\text{all2spaths}} p_{s2}p_{\text{ns3}a}p_{\text{ap}} + \cdots\right], \quad (1)$$

where I_0 is the intensity of the source, and p_{s1} is the probability of a particular single-scattering path that hits the detector. The probability that the photon was not scattered off the path and the photon was not absorbed along its path is $p_{\text{ns2}a}$. Finally, p_{ap} is the probability that the photon is within the numerical aperture of the detector and is thus counted. Similarly, p_{s2} is the probability of a particular two-scattering path that hits the detector and $p_{\text{ns3}a}$ is the probability that the photon is not scattered a third time along that path or absorbed. This series continues and includes paths with infinite numbers of scatterings, but $p_{\text{nsZ}a}$ decreases when the number of scatterings Z and hence the photon path length over which absorption occurs, becomes large. This factor limits the contribution of later terms.

While individual scattering events in the tissue are anisotropic, if absorption is sufficiently high and the source-detector separation is small, most of the detected photons re-

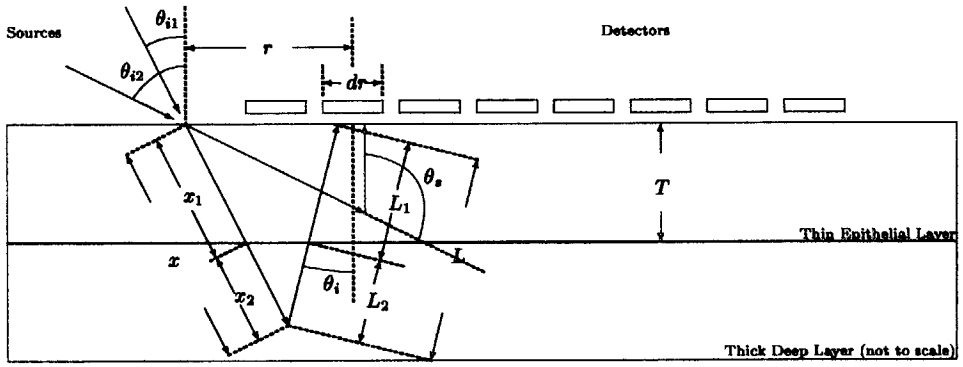

Fig. 1 Two-dimensional rendition of the 3-D oral model showing two angles of insertion and a detector at offset r.

verse their direction only once.[19] For the oral epithelium, we are interested in source-detector separations between 0.1 and 0.5 mm, which is less than $0.5/\mu_s'$. The transport-corrected scattering coefficient $\mu_s'=\mu_s(1-g)$, where μ_s is the inverse mean distance between scattering events and for this work has units of inverse millimeters and g is the coefficient of anisotropy, which is the mean cosine of the scattering angle. At these small separations, the behavior can be characterized as a single isotropic scattering event by rescaling the tissue properties so that an isotropic model can be used.

Our single-scattering oral model corresponds to the first term in Eq. (1) and includes two layers. The first and upper model layer, which mimics the epithelial layer, has high scattering and low absorption. The second, deeper layer, which models the stroma, has lower scattering, but much higher absorption (same order as the corrected scattering coefficient). Photons entering the medium have differing probabilities of being scattered back to the detectors according to the optical properties of each layer and the thickness of the first layer. The thickness of the second layer is assumed to be infinite, which is reasonable given its high absorption coefficient and the small source-detector separations.

In the scattering geometry illustrated in Fig. 1, the photons enter the tissue at a specific angle and travel in a roughly straight trajectory. The photons may experience numerous small-angle scatterings that have negligible effect on the initial trajectory. Each of the detected photons will have experienced one large-angle, direction-reversing scattering at the photon's maximum penetration depth. That is followed by multiple small-angle scatterings during the transit to the tissue surface where a detector measures the photon's offset r from the insertion point.

To extract the depth from the intensity measurements, a theory of photon propagation through the tissue to the detectors is required. First we will expand the probabilities in the first term of Eq. (1). The first probability p_{s1} is the product of two terms describing the probability of scattering at a point in the tissue and the probability that the scattering will result in a trajectory that hits a detector. The probability of a scattering event in a small interval dx at point x in the top layer is

$$p_{sL1}(x)=\mu_{s1}'\exp[-(\mu_{s1}'+\mu_{a1})x_1]\,dx, \tag{2}$$

where μ_{s1}' and μ_{a1} are the transport-corrected scattering and absorption coefficients for the top layer. In this layer, $x_1=x$ is the photon path length that corresponds to the distance from the insertion point along the insertion vector to the scattering point. If the scattering occurs in the deep layer, the formula becomes

$$p_{sL2}(x)=\mu_{s2}'\exp[-(\mu_{s1}'+\mu_{a1})x_1]\times\exp[-(\mu_{s2}'+\mu_{a2})x_2]\,dx, \tag{3}$$

where μ_{s2}' and μ_{a2} are the scattering and absorption coefficients for the bottom layer, x_2 is the path length in the deep layer, and $x_1+x_2=x$.

The probability that the scattering sends the photon in the direction of a detector located at offset r with small area $dr\,dw$ is

$$p_{\theta,\phi}(x,r,\theta_i)=\frac{dr\,dw\cos(\theta_a)}{4\pi L^2}, \tag{4}$$

where θ_i is the insertion angle of the source from the surface normal, and θ_a is the angle of arrival at the detector, which is a function of x, r, and θ_i. The path length L is from the scattering point to the detector; L is also dependent on x, θ_i, and θ_a.

The probability of a photon not being absorbed or scattered along the path from the first scattering point to the detector must be broken into two parts. The first equation is for scattering that occurs in the top layer:

$$p_{\mathrm{ns2}aL1}(x,r,\theta_i)=\exp[-(\mu_{s1}'+\mu_{a1})L_1], \tag{5}$$

where L_1 is the path length in the top layer from the scattering point to the detector. When the scattering occurs in the deep layer the expression becomes

$$p_{\mathrm{ns2}aL2}(x,r,\theta_i)=\exp[-(\mu_{s1}'+\mu_{a1})L_1]\times\exp[-(\mu_{s2}'+\mu_{a2})L_2], \tag{6}$$

where L_2 is the part of the path length from the scattering point to the detector, which is in the deep layer and $L_1+L_2=L$.

If the photon arrival at the detector is at too great an angle, the photon will not be captured by the detector. Generally, this is described by the numerical aperture of the detector, which is defined as the sine of the half-angle in which photons are

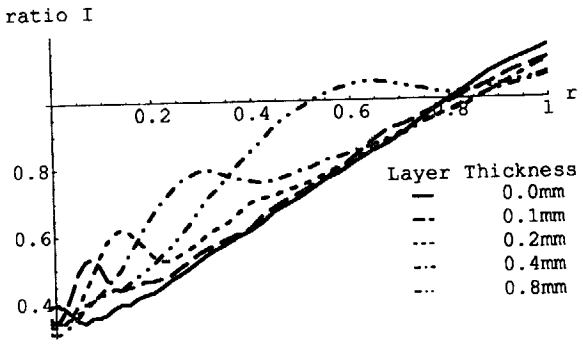

Fig. 2 Ratio of the intensities from two source insertion angles (22 deg/42 deg) as a function of source-detector separation r from MC simulations for epithelial layer thicknesses from 0.0 to 0.8 mm with top layer $\mu_s'=0.3$/mm, bottom layer $\mu_s'=0.15$/mm, top layer $\mu_a=0.07$/mm, bottom layer $\mu_a=0.35$/mm, and $g=0.7$.

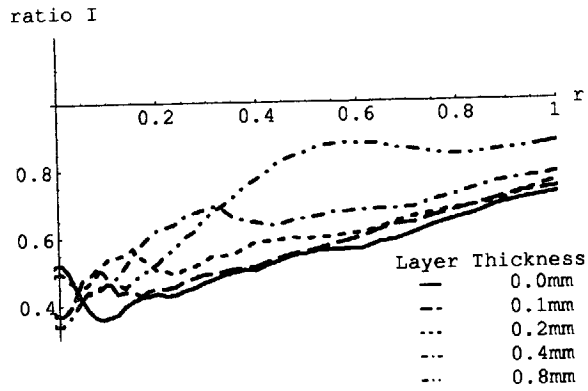

Fig. 3 Ratio of the intensities from two source insertion angles (22 deg/42 deg) as a function of source-detector separation r from MC simulations for epithelial layer thicknesses from 0.0 to 0.8 mm with top layer $\mu_s'=0.3$/mm, bottom layer $\mu_s'=0.15$/mm, top layer $\mu_a=0.007$/mm, bottom layer $\mu_a=0.035$/mm, and $g=0.7$.

captured. That half-angle is measured from the surface normal to the largest angle at which a photon will be captured by the detector. A numerical aperture term is included for the DRS in which

$$p_{\text{ap}}(x,r,\theta_i)=0 \quad \text{for} \quad \sin(\theta_a)>\text{numerical aperture} \tag{7}$$

$$p_{\text{ap}}(x,r,\theta_i)=1 \quad \text{for} \quad \sin(\theta_a)\leq\text{numerical aperture}. \tag{8}$$

Combining Eqs. (2) through (8), we obtain

$$I_d(r)\approx I_0\Bigg[\int_0^{\text{layer1}} p_{sL1}(x)p_{\theta,\phi}(x,r,\mathrm{d}r,\mathrm{d}w,\theta_i) \times p_{\text{ns2}aL1}(x,r,\theta_i)p_{\text{ap}}(x,r,\theta_i)\,\mathrm{d}x + \int_{\text{layer1}}^{\text{layer2}} p_{sL2}(x)p_{\theta,\phi}(x,r,\mathrm{d}r,\mathrm{d}w,\theta_i) \times p_{\text{ns2}aL2}(x,r,\theta_i)p_{\text{ap}}(x,r,\theta_i)\,\mathrm{d}x\Bigg], \tag{9}$$

where layer1 is the point on the insertion vector where it crosses from the top layer to the bottom layer. Similarly,

Table 1 Intensity ratio peak offsets (mm).

	Top Layer			Layer Thickness			
Type	μ_s' (mm^{-1})	g	μ_a (mm^{-1})	0.1 mm	0.2 mm	0.4 mm	0.8 mm
MC	0.3	0.07	0.7	0.074	0.133	0.309	0.641
MC	0.3	0.007	0.7	0.074	0.148	0.309	0.578
Theory	0.3	0.0	0.0	0.065	0.135	0.265	0.515
MC	0.6	0.07	0.7	0.074	0.148	0.329	0.675
MC	0.6	0.007	0.7	0.060	0.149	0.329	0.641
Theory	0.6	0.0	0.0	0.065	0.135	0.255	0.505
MC	1.2	0.07	0.7	0.074	0.164	0.350	0.832
MC	1.2	0.007	0.7	0.074	0.180	0.350	0.675
Theory	1.2	0.0	0.0	0.065	0.125	0.245	0.475
Phantom	1.2	0.07	0.7	0.10	0.20	0.40	0.40

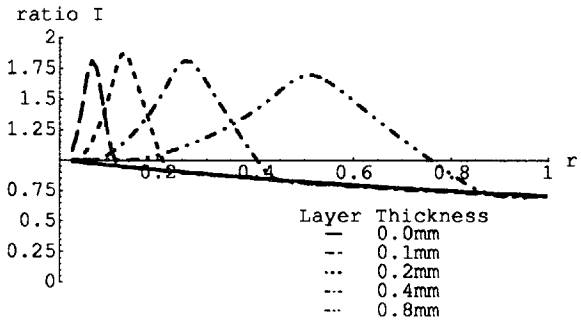

Fig. 4 Ratio of the intensities from two source insertion angles (22 deg/42 deg) as a function of source-detector separation r from theory for epithelial layer thicknesses from 0.0 to 0.8 mm with top layer μ_s =0.3/mm and bottom layer μ_s=0.15/mm normalized to an infinite layer with μ_s=0.3/mm.

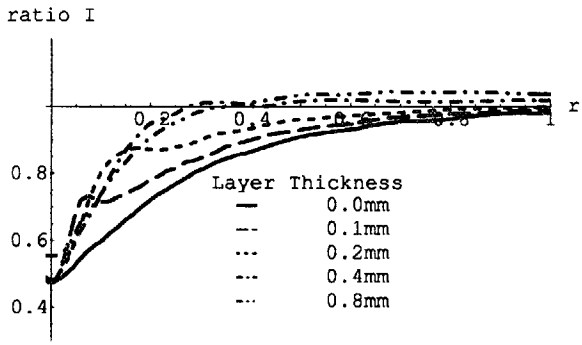

Fig. 6 Ratio of the intensities from two source insertion angles (22 deg/42 deg) as a function of source-detector separation r from MC simulations for epithelial layer thicknesses from 0.0 to 0.8 mm with top layer μ_s'=1.2/mm, bottom layer μ_s'=0.6/mm, top layer μ_a =0.007/mm, bottom layer μ_a=0.035/mm, and g=0.7.

layer2 is the point on the insertion vector where it exits the bottom layer, which, due to the high absorption coefficient, is effectively infinity for our bottom layer.

If two or more sources are used at different insertion angles, and the ratio of intensities is computed, the dependence on absolute source intensity I_0 in Eq. (9) can be removed. Additionally, the intensity ratio provides a sensitive method for highlighting small differences in intensities that arise from the two insertion angles.

3 MC Simulation and Phantom Methods

We compare the predictions from our theory with MC simulations and phantom experiments. To obtain the high absorption required for a single scatter model, 532-nm wavelength light (which is near peak hemoglobin absorption wavelengths) is used. The parameters used in the simulations are intended to mimic the optical properties of tissue, but also match those of the phantoms. Thus, while tissue typically has $g \approx 0.9$ the simulations were run with $g=0.7$ to match measured values in our phantoms.

The phantoms were gel-based with intralipid added for scattering and were similar to those described by Wagnieres et al.[22] The phantoms were imaged using free-space optics lasers and a high-dynamic range imager. The photon insertion angle was corrected for refraction at the surface. Due to the difficulty of manufacturing precise life-scale layered phantoms, the phantoms were manufactured 10× scale with scaled optical properties. The results are scaled down to equivalent life-scale for comparison with MC simulations and to provide an indication of life-scale performance.

In MC simulations, a photon is initiated at the tissue surface with the desired insertion angle. Random draws determine the distance the photon travels before being scattered. Another random draw determines the scattering angle. This sequence is continued until specific exit criteria are met such as the photon hitting a detector. If an enormous number of individual photons are run in such a manner and their exit positions are combined, the statistics resemble those of a beam of light. This provides a powerful tool to investigate the behavior of photons in very well characterized scattering media.

The MC simulation used in this research enables the user to vary the photon insertion angle and to select the thickness of each layer and the scattering characteristics μ_s and g of each of the layers. Unlike the theory, the MC simulations employ anisotropic scattering and the detected photons have typically experienced a minimum of several scattering events. Compared to Mie scattering from identical spheres, the Henyey-Greenstein phase function has both increased forward and backscattering probabilities, which better matches scatter-

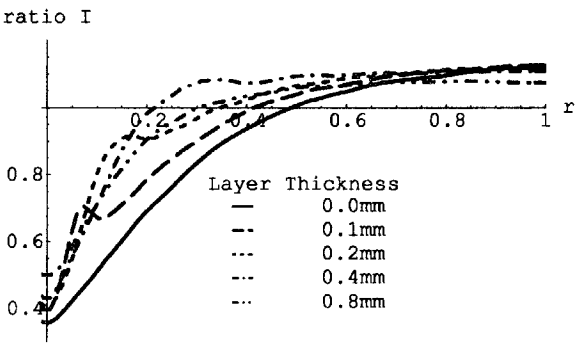

Fig. 5 Ratio of the intensities from two source insertion angles (22 deg/42 deg) as a function of source-detector separation r from MC simulations for epithelial layer thicknesses from 0.0 to 0.8 mm with top layer μ_s'=1.2/mm, bottom layer μ_s'=0.6/mm, top layer μ_a =0.07/mm, bottom layer μ_a=0.35/mm, and g=0.7.

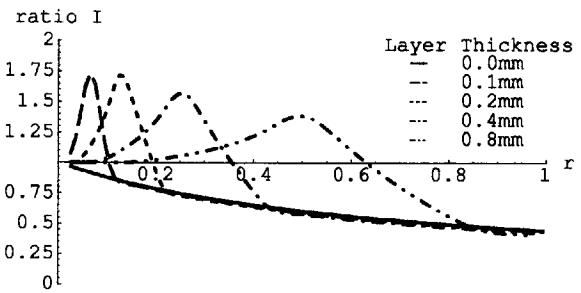

Fig. 7 Ratio of the intensities from two source insertion angles (22 deg/42 deg) as a function of source-detector separation r from theory for epithelial layer thicknesses from 0.0 to 0.8 mm with top layer μ_s =1.2/mm and bottom layer μ_s=0.6/mm normalized to an infinite layer with μ_s=1.2/mm

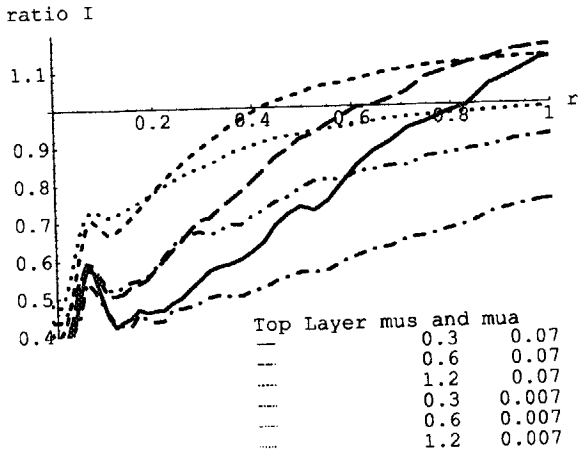

Fig. 8 Ratio of the intensities from two source insertion angles (22 deg/42 deg) as a function of source-detector separation r from MC simulations for fixed epithelial layer thickness of 0.1 mm for $\mu_s' = 0.3$, 0.6, and 1.2/mm; $\mu_a = 0.07$ and 0.007/mm; and $g = 0.7$.

ing from the broad range of scatterer sizes found in tissue and was therefore used in the simulations. Since each photon has typically experienced several scatterings, the dependence of the results on peculiarities of a particular phase function are reduced.

Each layer may have a different index of refraction, which determines the probability of a photon being reflected at a boundary or crossing a layer boundary with its attendant change in angle. The length of the path traveled in each layer by a photon is recorded for all photons exiting at a detector location. This enables the effect of absorption to be calculated retrospectively. A maximum of 300 scatterings were allowed in the presented results and a maximum photon path length of 25 mm. Photons exceeding these parameters were dropped to reduce computational time. From parametric trials it was determined that these limiting values are large enough that the resulting errors are negligible.

4 MC Simulation and Phantom Results

The ratio of intensities from MC simulations for two tissue insertion angles, 22 and 42 deg, were computed for each source-detector distance as shown in Figs. 2 to 5. Unlayered scattering media are generally characterized by a log-linear decrease in intensity as a function of distance from a light source. The ratio of intensities from two sources at different angles relative to the tissue surface generally results in a monotonically increasing ratio as a function of offset. For low scattering coefficients compared to typical tissue ($\mu_s' = 0.3$/mm, $g = 0.7$, and relatively high absorption, $\mu_a = 0.35$/mm), the monolayer shows a minimum near 0.1-mm offset, as we can see in Fig. 2. At lower absorptions, MC simulations show that the minimum in the monolayer is more well defined and the average slope of the intensity ratio is smaller.

For layered structures, the intensity ratio exhibits a distinctive local maximum at a source-detector distance proportional to layer thickness similar to those previously reported for isotropic scattering.[21] When absorption is reduced by a factor of 10 to bracket what would be expected in tissue, the peaks are still distinctive as we can see in Fig. 3 and the slope of the intensity ratio decreases as described for the mono-layer case. The distances of the peaks shown in Figs. 2 and 3 from the origin are listed in Table 1.

Equation (9) can be used to compute the same ratios. At distances greater than approximately 0.5 mm, there is an exponentially increasing bias error resulting from omission of multiple scattering. To facilitate comparisons between theory and MC simulations, the theory predictions were normalized by the prediction for a single layer with the scattering properties of the top layer. The theory results are shown in Fig. 4. Note also that for the isotropic scattering in the theory, $g = 0$ and $\mu_s' = \mu_s$. The radial peak locations are listed in Table 1 and can be seen to be approximately the same as for the MC simulations. At very small source-detector distances, we expect an error due to g.

Those two sources of error change the global shape of the theory predictions. Because of their small spatial extent, the local maxima corresponding to particular layer thicknesses are preserved in the presence of those errors. The narrow peak for our shallowest layer boundary is very accurately described by the single isotropic scattering theory. We can see in Figs. 2 and 3 that the peak for the 0.8-mm layer is broadened. This broadening makes localization of the peak difficult and is hence a source of layer thickness quantification error.

Increasing the scattering results in monolayers having a monotonically increasing intensity ratio value. Layered media retain the distinctive local maxima. For thicker layers of 0.4

Table 2 Peak location mean [mm] and variance of data in Table 1 for various layer thicknesses.

	Layer Thickness							
	0.1 mm		0.2 mm		0.4 mm		0.8 mm	
Data	Mean	σ^2	Mean	σ^2	Mean	σ^2	Mean	σ^2
MC	0.717	3.27×10^{-5}	0.154	2.63×10^{-4}	0.329	3.36×10^{-4}	0.674	7.27×10^{-3}
Theory	0.650	0.00	0.132	3.33×10^{-5}	0.255	1.00×10^{-4}	0.498	4.33×10^{-4}
Theory Error	9.30%		14.3%		22.6%		26.0%	

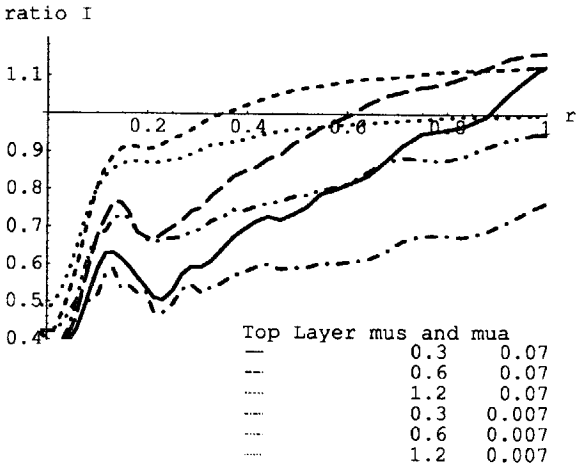

Fig. 9 Ratio of the intensities from two source insertion angles (22 deg/42 deg) as a function of source-detector separation r from MC simulations for fixed epithelial layer thickness of 0.2 mm for μ_s' =0.3, 0.6, and 1.2/mm; μ_a=0.07 and 0.007/mm; and g=0.7.

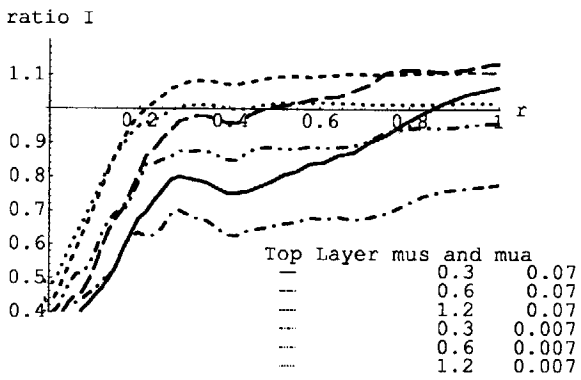

Fig. 10 Ratio of the intensities from two source insertion angles (22 deg/42 deg) as a function of source-detector separation r from MC simulations for fixed epithelial layer thickness of 0.4 mm for μ_s' =0.3, 0.6, and 1.2/mm; μ_a=0.07 and 0.007/mm; and g=0.7.

and 0.8 mm, the peak is broader than for the lower scattering case. Further increasing the scattering to $\mu_s'=1.2$/mm accentuates the flattening of the slope at large source-detector separations which results in more curvature of the ratios. We can see this clearly in the monolayer plots in Figs. 5 and 6. At this level of scattering, the broadening of the peaks for the 0.4- and 0.8-mm layers is also very evident.

This indicates that a method relying on localization of the peak for quantization of layer thickness will lose precision for thicker layers in higher scattering media. The sharpness of the peaks for thinner layers corresponding to healthy and moderately inflamed tissue, however, remain distinct even with high scattering. For this level of scattering, the match in the peak locations between Figs. 5 and 6 and the theory is good only for the 0.1- and 0.2-mm-thick layers, as we can see in Fig. 7. The loss in localization due to multiple scattering has significantly broadened the 0.4- and 0.8-mm peaks relative to the theory.

Figure 8 plots the intensity ratios for a fixed 0.1-mm layer thickness with varying scattering and absorption, including all MC cases shown in Figs. 3 through 5, as well as an intermediate case with top layer $\mu_s'=0.6$/mm. For the 0.1-mm layer thickness, the location of the peak maxima is very consistent (variance is approximately 3.27×10^{-5} as shown in Table 2). Similarly, Figs. 9 and 10 show the robustness of the location of the peak maximum to changes in scattering and absorption for fixed layer thicknesses of 0.2 and 0.4 mm, respectively. For layer thicknesses ranging from 0.1 to 0.4 mm, peak maximum location variance increases with increasing layer thickness and is less than 3.36×10^{-4} despite a fourfold change in the scattering coefficient and a 10-fold change in the absorption coefficient. Thus, knowledge of tissue optical characteristics is not necessary for quantification of layer thickness, given a clear local maximum in the intensity ratio.

Given the simplicity of the theory, layer thickness could be rapidly obtained by iterative computation of the theory until a matching layer peak location is obtained. Using such a method and ignoring what appears to be a linear error between the theory and MC results, such a method would be expected to have a mean error less than 30%, as we can see in Table 2. The error increases as layer thickness increases, which suggests a correction factor could be used to improve performance. Further, typical patient layer thicknesses correspond to a mean error of less than 10%. Alternatively, an empirical method may be used by noting that the peak location in the MC data occurs at approximately 0.75 the epithelial layer thickness. In any case, even with a mean error of 30%, the method provides a potentially useful clinical measure since our histological data show epithelial thickness can be over 400% greater than normal in patients with risk factors for developing cancer such as leukoplakia.

A set of phantoms, with optical characteristics approximately those of the most difficult case of high scattering shown in the MC simulation results in Fig. 5, were imaged. In Fig. 11, the local intensity ratio maxima for 0.1- and 0.2-mm thickness layers are evident, whereas the location of the intensity peak maxima for the thicker 0.4- and 0.8-mm layers are much less distinct. The peak locations in the phantom are consistently approximately 30% larger than seen in the theory and MC simulations.

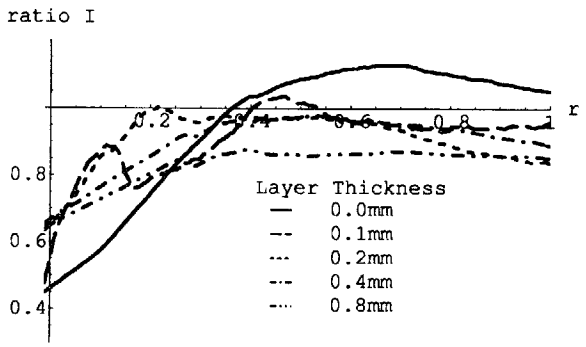

Fig. 11 Ratio of the intensities from two source insertion angles (22 deg/42 deg) as a function of source-detector separation r from phantom experiments for epithelial layer thicknesses from 0.0 to 0.8 mm with scattering and absorption approximately those in Fig. 5.

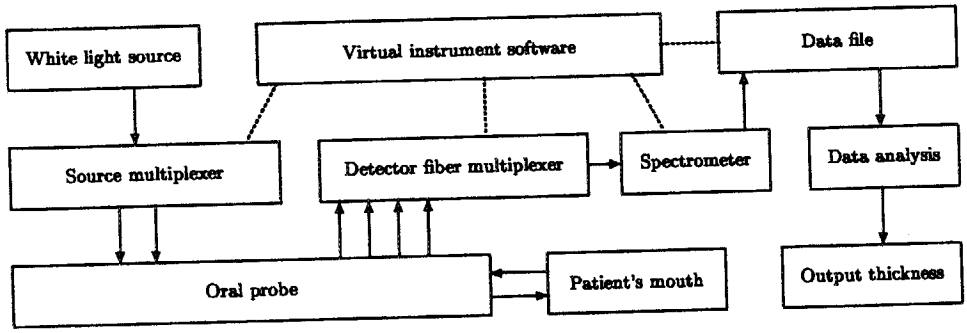

Fig. 12 Block diagram of oral DRS device showing how white light is transmitted to the patient and the reflected light is processed into a measure of epithelial thickness.

5 Clinical Measurement Methods

A system based on the block diagram in Fig. 12 was built and tested in a clinical trial evaluating the effectiveness of an oral rinse containing a Cox inhibitor. Patients in the study had a premalignant condition of the mouth called leukoplakia. Punch biopsies were taken of patients in the study, but those sites were not coincident with DRS measurement sites. Biopsies were taken at several locations and showed that patients with lesions had significant heterogeneity in epithelial thickness and inflammation throughout the oral cavity, not only near the lesion sites. The intent of our involvement in the clinical study was to assess the ability of a very simple DRS probe to distinguish a difference between patients and controls. Additionally, DRS measurements were not taken at sites with visually evident lesions. This was so because clear visual indications of inflammatory processes do not require a DRS device. Inflammation without clear visual indications is where DRS is valuable.

In this simple probe, input light is supplied by two switched tungsten halogen lamps. The tungsten halogen lights are directed to the tissue surface by fiber optics such that one lamp provides light at an oblique angle of 60 deg to the tissue surface normal and the other at 30 deg. The lamps are switched so that only one is on at a time. Light is delivered to the tissue by a probe that holds the fibers in proper alignment with the tissue surface, as shown in Fig. 13. The probe has a tissue contact area containing the fibers that is just over 1 cm long and is manipulated using a 15-cm-long handle. Light passes through the tissue and is collected by four receiver/detector fibers in the probe that are multiplexed into a spectrometer. Thus, in this design, the desired wavelength can be selected after data collection.

6 Preliminary Clinical Results

Since the probe measures only four spatially resolved positions, identification of the increase in intensity ratios shown in Figs. 2 to 10 is not possible. For the clinical work, a simple feature that indicated an approximate level of inflammation was desired. As we can see in the MC simulation plots, the intensity ratios converge to the same value at large source detector separations regardless of layer thickness (Fig. 14). Thus, we used the largest source-detector separation on the probe, 3.8 mm, as a normalizing reference. The smallest source-detector separation in the probe was 0.8 mm. This corresponds to the peak intensity ratio of an epithelial layer 0.8 mm thick, and where there is large variation in intensity as a function of layer thickness, as we can see in Fig. 14.

Clinically, we expect that all patients will have significantly smaller epithelial thicknesses even with very high levels of inflammation. Our clinical feature was obtained by taking the smallest source-detector intensity ratio and dividing it by the largest source-detector ratio. This ratio of ratios is smallest for small layer thicknesses and largest for large layer thicknesses up to 0.8 mm. This feature is highly variable, depending on the location and shape of the intensity ratio peak. Thus, the actual feature value is very nonlinear compared to the intensity peak location used with the very high spatial resolution MC simulation and phantom data.

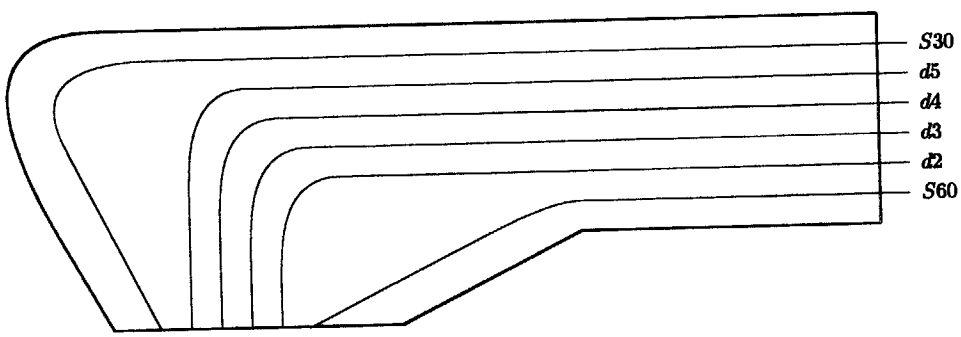

Fig. 13 Oral DRS probe diagram showing position of four detector fibers, $d2$ through $d5$, and two source fibers, $S30$ and $S60$, which are angled 30 and 60 deg, respectively, from the tissue surface normal.

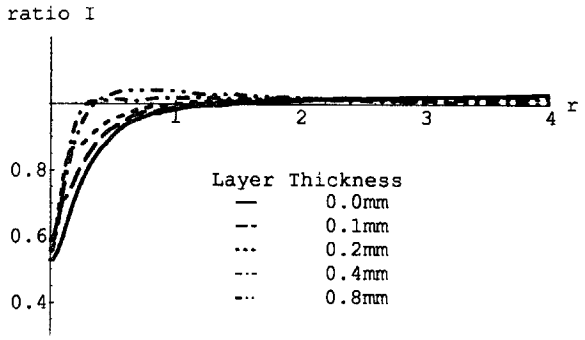

Fig. 14 Same plot as Fig. 6 except extended out to source-detector separation of 4 mm to show convergence.

Figure 15 clearly shows that the feature is lowest for the healthy controls. This is consistent with the absence of inflammation. Hemoglobin has large absorption peaks at approximately 540 and 575 nm. Most patients have small dips in their feature value near these peaks, as we can see in Fig. 15. Since errors due to multiple scattering will be smallest at these wavelengths, the ratios there are used. The feature value is consistent over a large range of absorption coefficients, which indicates the robustness of the technique.

7 Conclusion

Inflammation of the oral epithelium contributes to the pathogenesis of oral cancer. The development of new chemopreventive drugs requires monitoring of oral inflammation; typically, the monitoring is performed via invasive biopsy. We have developed a noninvasive optical technique based on DRS. MC simulations show that diffusely reflected photons in a tissue-like, highly scattering and absorbing medium can be used to characterize the optical properties of tissue within 1 mm of the surface. The basis of the method is a single-scattering theory. This theory has known limitations at very small source-detector separations due to anisotropic scattering in tissue. Additionally, multiple scattering invalidates the theory for large source-detector separations and when absorption is low. We identified a feature that exists at intermediate distances where the theory is valid; additionally, wavelengths are used where absorption in tissue is high.

A ratio of intensities from two sources at different angles relative to the tissue surface provides a measure of intensity that is independent of absolute intensity. For the chosen insertion angles, MC simulations predict that the intensity ratio will have a local maximum at a source-detector distance equal to approximately 0.75 of the epithelial layer thickness. The locations of the peaks are very robust to changes in the scattering and absorption coefficients that would be expected in a diverse pool of human subjects. The variance in peak location increases as layer thickness increases. This is caused by broadening of the peaks due to multiple scattering. For layer thicknesses expected in normal to inflamed epithelial thicknesses of 0.1 to 0.4 mm, the variance in peak location is less than 3.36×10^{-4}. This, combined with phantom experiments, indicates that the approach is a simple, yet effective, method for quantifying epithelial thickness *in vivo* with an error less than 30% despite a fourfold change in scattering coefficients and a 10-fold change in absorption coefficients. Given that oral inflammation can increase epithelial thickness by 400%, this new method has potential application as a clinically useful tool. Clinical trials with a simple probe using a readily measured feature also show the promise of the technique.

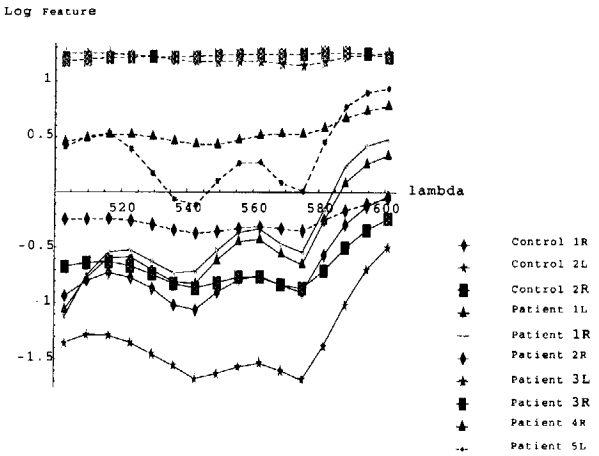

Fig. 15 Oral patient feature data/oral patient buccal mucosa feature data as a function of wavelength for two controls and four patients (some patients with measurements on both left and right sides).

References

1. L. M. Coussens, W. W. Raymond, G. Bergers, M. Laig-Webster, O. Behrendtsen, Z. Werb, G. H. Caughey, and D. Hanahan, "Inflammatory mast cells up-regulate angiogenesis during squamous epithelial carcinogenesis," *Genes Dev.* **13**, 1382–1397 (June 1999).
2. S. H. Hong, F. G. Ondrey, I. M. Avis, Z. Chen, E. Loukinova, P. F. C. Jr., C. V. Waes, and J. L. Mulshine, "Cyclooxygenase regulates human oropharyngeal carcinomas via the proinflammatory cytokine il-6: a general role for inflammation?" *FASEB J.* **14**, 1499–1507 (Aug. 2000).
3. C. Cordon-Cardo and C. Prives, "At the crossroads of inflammation and tumorigenesis," *J. Exp. Med.* **190**, 1367–1370 (Nov. 1999).
4. W. K. Hong and M. B. Sporn, "Recent advances in chemoprevention of cancer," *Science* **278**(5340), 1073–1077 (1997).
5. P. F. C. Jr., M. P. Meredith, W. Buchanan, M. J. Doyle, M. S. Reddy, and M. K. Jeffcoat, "Coordinate production of pge2 and il-1 beta in the gingival crevicular fluid of adults with periodontitis: its relationship to alveolar bone loss and disruption by twice daily treatment with ketorolac tromethamine oral rinse," *J. Lightwave Technol.* **33**, 75–82 (Feb. 1998).
6. M. Keijzer, W. M. Star, and P. R. M. Storchi, "Optical diffusion in layered media," *Appl. Opt.* **27**(9), 1820–1824 (1988).
7. H. Taitelbaum, S. Havlin, and G. H. Weiss, "Approximate theory of photon migration in a two-layer medium," *Appl. Opt.* **28**(12), 2245–2249 (1989).
8. M. A. Franceschini, S. Fantini, L. A. Paunescu, J. S. Maier, and E. Gratton, "Influence of a superficial layer in the quantitative spectroscopic study of strongly scattering media," *Appl. Opt.* **37**(31), 7447–7458 (1998).
9. T. J. Farrell, M. S. Patterson, and M. Essenpreis, "Influence of layered tissue architecture on estimates of tissue optical properties obtained from spatially resolved diffuse reflectometry," *Appl. Opt.* **37**(10), 1958–1972 (1998).
10. E. M. Sevick and B. Chance, "Photon migration in a model of the head measured using time- and frequency-domain techniques. potentials of spectroscopy and imaging," in *Proceedings of Time-Resolved Spectroscopy and Imaging of Tissues, Proc. SPIE* **1431**, 84–96 (Jan. 1991).
11. M. Ferrari, R. A. D. Blasi, S. Fantini, B. F. Barbieri, and E. Gratton, "Cerebral and muscle oxygen saturation measurement by a frequency-domain near-infrared spectroscopic technique," in *Progress in Biomedical Optics, Proceedings of Optical Tomography,*

Photon Migration, and Spectroscopy of Tissue and Model Media: Theory, Human Studies, and Instrumentation, Proc. SPIE **2389**, 868–875 (1995).
12. R. Nossal, R. Bonner, S. Havlin, and G. H. Weiss, "Photon migration in layered media," *Appl. Opt.* **27**, 3382–3391 (1988).
13. G. H. Weiss, R. Nossal, and R. F. Bonner, "Statics of penetration depth of photons re-emitted from irradiated tissue," *J. Mod. Opt.* **36**(3), 349–359 (1989).
14. I. Dayan, S. Havlin, and G. H. Weiss, "Photon migration in a two-layer turbid medium. a diffusion analysis," *J. Mod. Opt.* **39**, 1567–1582 (1992).
15. J. M. Schmitt, M. J. Yadlowsky, and R. F. Bonner, "Subsurface imaging of living skin with optical coherence microscopy," *Dermatology (Basel, Switz.)* **191**(2), 93–98 (1995).
16. L. L. Otis, M. J. Everett, U. S. Sathyam, and B. W. C. Jr., "Optical coherence tomography: a new imaging technology for dentistry," *J. Am. Dent. Assoc.* **131**, 511–514 (Apr. 2000).
17. C. Pitris, M. E. Brezinski, B. E. Bouma, G. C. Tearney, J. F. Southern, and J. G. Fujimoto, "High resolution imaging of the upper respiratory tract with optical coherence tomography: a feasibility study," *Am. J. Respir. Crit. Care Med.* **157**, 1640–1644 (May 1998).
18. J. M. Schmitt, G. X. Zhou, and E. C. Walker, "Multilayer model of photon diffusion in skin," *J. Opt. Soc. Am. A* **7**, 2141–2153 (Nov. 1990).
19. A. H. Gandjbakhche, R. F. Bonner, A. E. Arai, and R. S. Balaban, "Visible-light photon migration through myocardium in vivo," *Am. J. Physiol.* **277**, H698–H704 (Aug. 1999).
20. A. E. Arai, C. E. Kasserra, P. R. Territo, A. H. Gandjbakhche, and R. S. Balaban, "Myocardial oxygenation in vivo: optical spectroscopy of cytoplasmic myoglobin and mitochondrial cytochromes," *Am. J. Physiol.* **277**, H683–H697 (Aug. 1999).
21. D. Hattery, K. Gerdelman, F. Hekmat, V. Chernomordik, P. Smith, A. Eidsath, R. Pursley, J. Atkinson, J. Mulshine, and A. Gandjbakhche, "Diffuse reflectance spectroscopy to quantify inflamation of the oral epithelium in vivo," in *Progress in Biomedical Optics and Imaging: Optical Biopsy IV*, R. R. Alfano, Ed., *Proc. SPIE* **4613**, 59–70 (2002).
22. G. Wagnieres, S. Cheng, M. Zellweger, N. Utke, D. Braichotte, J. P. Ballini, and H. van den Bergh, "An optical phantom with tissue-like properties in the visible for use in pdt and fluorescence spectroscopy," *Med. Phys. Biol.* **42**, 1415–1426 (1997).